Advancements in Human-Cable Collision Detection and Management in Cable-Driven Parallel Robots

Hanbang Gao, Christine Chevallereau, Stéphane Caro

Advancements in Human-Cable Collision Detection and Management in Cable-Driven Parallel Robots

Hanbang Gao, Christine Chevallereau, and Stéphane Caro

Nantes Université, École Centrale Nantes, CNRS, LS2N, UMR 6004, F-44000 Nantes, France.
{hanbang.gao, christine.chevallereau, stephane.caro}@ls2n.fr

Abstract. This paper presents significant advancements in the detection and management of human-cable collisions within Cable-Driven Parallel Robots. Building upon previous research [1], A novel frequency-based filter is developed and applied to tension sensor measurements, enabling collision detection based on cable tension measurements. This approach facilitates the identification of the colliding cable and allows for the reduction of the concerned cable tension, permitting safe contact between the cable and the environment or operator without causing damage. Additionally, a robust method for detecting the end of collisions is proposed, ensuring the system can promptly return to normal operation. An adaptive control method for cable length release is also developed, optimizing collision management during dynamic human-robot interactions. The proposed management approach effectively handles both severe and minor collisions. Experiments conducted with the CRAFT prototype validate these improvements, demonstrating that they substantially enhance safety and responsiveness in physical human-robot collaboration, thereby marking a noteworthy progression in collaborative robotic environments.

Keywords: Tendon/wire mechanism · Parallel robots · Human-robot collaboration · Physical human-robot interaction · Safety in HRI.

1 Introduction

Collaborative Cable-Driven Parallel Robots (CDPRs) have gained attention in industrial applications for their large workspaces and high-speed capabilities [2]. Despite these advantages, the risk of human-cable collisions raises serious safety concerns, making their deployment challenging in human-robot collaborative environments. Traditional CDPRs often rely on restrictive safety measures, which significantly limit their usability.

Efforts to enhance safety in CDPRs have centered on advancements in design and control strategies. Reconfigurable CDPRs (RCDPRs) aim to reduce collision risks by modifying cable exit points and cable anchor points, which serve as the connections between cables and the robot's base frame [3]. Another

innovative approach involves movable anchor winch systems (MCDPRs), where winches travel along tracks to improve obstacle avoidance and facilitate seamless cooperation among multiple robots [4]. When collisions cannot be fully avoided, studies on geometric and kinematic modeling of cable wrapping offer strategies for controlled cable behavior. This includes adaptive designs for unlimited rotation axes [5], analysis of cable statics and paths [6], and extended kinematic control for cable wrapping on various geometries [7].

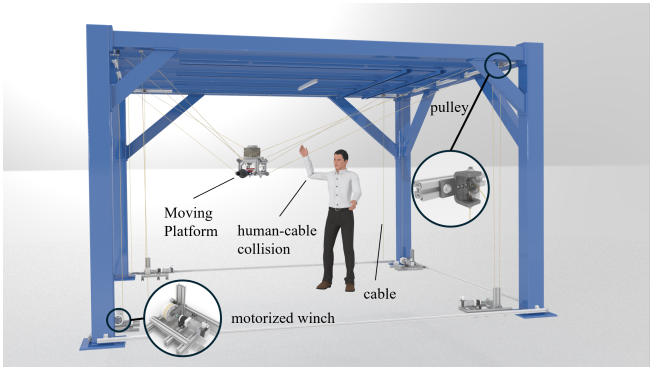

Fig. 1: Prototype of the CRAFT system and human-cable collision case

Human-cable collision, as shown in Fig. 1, was studied for CDPRs in [8], where a cable release strategy was proposed. Gao et al. [1] expanded on this research by employing tension sensors and motor encoders to detect and manage collisions, initiating cable release upon detection. Although effective, these methods may face challenges in response time and precision during dynamic interactions.

Building on prior approaches, this work integrates a frequency-based filtering mechanism to improve collision detection speed and precision, and adopts adaptive cable release methods to address actuator non-reversibility. These enhancements strengthen tension regulation, ensuring safer and more efficient human-robot collaboration in CDPR systems.

2 Experimental Setup and Control Architecture

2.1 Experimental Setup

The CRAFT platform is an experimental CDPR prototype developed at LS2N. It features eight cables, each leading to a loop-closure equation. Every loop integrates a winch unit, a guiding pulley, and a cable that connects to the Moving Platform (MP). Fig. 1 illustrates one complete actuation chain within the CRAFT prototype. In this arrangement, the cable is wound around a drum, passes through a pulley, and then attaches to the anchor point on the MP.

The CRAFT platform uses a supervision PC linked to a real-time PC (via dSPACE) to control eight motors. Two sensor types provide feedback: motor encoders measure joint angles $\mathbf{q}$, and tension sensors near cable attachments measure tensions $\boldsymbol{\tau}_m$. Both are sampled at 1000 Hz.

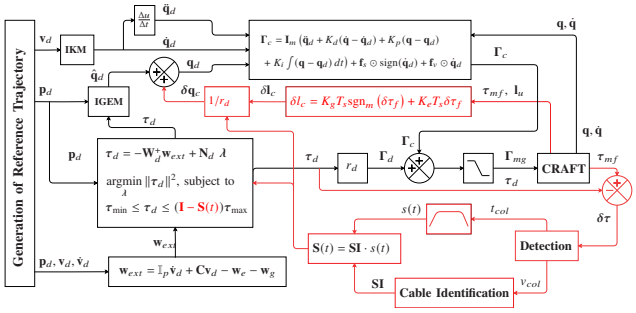

Fig. 2: Control scheme of the CRAFT platform: the red components represent the proposed collision management.

2.2 Control Scheme of CRAFT

The black blocks in Fig. 2 illustrate the CRAFT control scheme, which applies the motor-gearbox torque $\boldsymbol{\Gamma}_{mg}$ to achieve the desired pose $\mathbf{p}_d$, twist $\mathbf{v}_d$, and twist derivative $\dot{\mathbf{v}}_d$. This torque results from the combination of joint-space control $\boldsymbol{\Gamma}_c$ and cable tension management $\boldsymbol{\Gamma}_d$, with a saturation filter safeguarding the motor-gearbox against excessive forces.

The torque $\boldsymbol{\Gamma}_c$ follows a computed torque control law with a PID corrector, driving the motors from measured positions $\mathbf{q}$ to the desired $\mathbf{q}_d$. These desired positions are obtained via the Inverse Geometric Elasto-static Model (IGEM) [9], which considers pulley geometry and cable elasticity for precise motor control.

The PID corrector employs gains K_p, K_i, and K_d, selected to ensure that the closed-loop tracking error for the motor joints, $\mathbf{e} = \mathbf{q}_d - \mathbf{q}$, as described by the following equation, converges to zero:

$$\ddot{\mathbf{e}} + K_d\ \dot{\mathbf{e}} + K_p\ \mathbf{e} + K_i \int \mathbf{e}, dt = 0 \tag{1}$$

This control strategy minimizes the tracking error, thereby enhancing the accuracy and stability of motor joint movements within the CDPR system. The corresponding motor joint acceleration is:

$$\ddot{\mathbf{q}} = \ddot{\mathbf{q}}_d + K_d\ (\dot{\mathbf{q}} - \dot{\mathbf{q}}_d) + K_p\ (\mathbf{q} - \mathbf{q}_d) + K_i \int (\mathbf{q} - \mathbf{q}_d)\, dt \tag{2}$$

The torque $\boldsymbol{\Gamma}_c$ required to produce this acceleration compensates for Coulomb and viscous friction, modeled with static friction $\mathbf{f}_s$ and fluid friction $\mathbf{f}_v$:

$$\boldsymbol{\Gamma}_c = \mathbf{I}_m \ddot{\mathbf{q}} + \mathbf{f}_s \odot \operatorname{sign}(\dot{\mathbf{q}}_d) + \mathbf{f}_v \odot \dot{\mathbf{q}}_d, \tag{3}$$

where $\mathbf{I}_m$ is the inertia matrix of the motor and gearbox, and $\mathbf{a} \odot \mathbf{b}$ denotes element-wise multiplication of vectors $\mathbf{a}$ and $\mathbf{b}$.

The torque $\boldsymbol{\Gamma}_d$ calculates the motor torques required for the MP to follow desired trajectories by determining the desired cable tensions $\boldsymbol{\tau}_d$. It incorporates a feed-forward component $\mathbf{w}_{ext}$ from the Inverse Dynamic Model (IDM), which compensates for system dynamics, including inertia, Coriolis forces, and gravitational effects. This compensation is achieved without necessitating external measurements of the MP pose, velocity, and acceleration:

$$\mathbf{w}_{ext} = \mathbb{I}_p \dot{\mathbf{v}}_d + \mathbf{C}\mathbf{v}_d - \mathbf{w}_e - \mathbf{w}_g, \tag{4}$$

where $\mathbb{I}_p$ is the MP's inertia tensor, and $\mathbf{C}$, $\mathbf{w}_e$, and $\mathbf{w}_g$ denote the Coriolis matrix, external wrench exerted on the MP, and gravity wrench, respectively.

The desired cable tensions $\boldsymbol{\tau}_d$ are optimized using quadratic programming to determine a tension distribution within operational limits. In this study, the torque norm is minimized; nevertheless, alternative criteria can also be applied. The corresponding optimization problem is formulated as follows [1]:

$$\underset{\boldsymbol{\lambda}}{\operatorname{argmin}} \left\| \boldsymbol{\tau}_d \right\|^2, \quad \text{subject to} \quad \boldsymbol{\tau}_{\min} \leq \boldsymbol{\tau}_d \leq \boldsymbol{\tau}_{\max}. \tag{5}$$

Here, $\boldsymbol{\tau}_{\min}$ and $\boldsymbol{\tau}_{\max}$ represent the minimum (1 N) and maximum (100 N) cable tension vectors, ensuring cable tautness and safety, respectively. The desired cable tensions $\boldsymbol{\tau}_d$ for an eight-cable CDPR in a three-dimensional workspace are expressed as:

$$\boldsymbol{\tau}_d = -\mathbf{W}_d^{+} \mathbf{w}_{ext} + \mathbf{N}_d \boldsymbol{\lambda}, \tag{6}$$

where $\mathbf{W}_d$ is the desired wrench matrix (IGEM-based), $^+$ is the Moore-Penrose pseudo-inverse, and $\mathbf{N}_d$ is the null space of $\mathbf{W}_d$, satisfying $\mathbf{W}_d \mathbf{N}_d \boldsymbol{\lambda} = \mathbf{0}_6$. Using Eqs. (2)-(6), the motor torque control input is:

$$\boldsymbol{\Gamma}_{mg} = \operatorname{sat}(r_d \boldsymbol{\tau}_d + \boldsymbol{\Gamma}_c), \tag{7}$$

where $\operatorname{sat}(\cdot)$ is the saturation function, and r_d is the winch radius.

2.3 Experimental Trajectory

Two trajectories were designed to evaluate system performance under different conditions:

Static Trajectory: The MP remains stationary directly above the stand with servo motors activated. This setup serves as a baseline to assess collision detection and management without dynamic movements.

Dynamic Trajectory: A square trajectory with 1 m sides is executed over 60 seconds at an average speed of 0.1 m/s. The path is divided into eight phases to ensure smooth acceleration and prevent abrupt changes. A fifth-order polynomial motion plan precisely controls the MP position, velocity, and acceleration, facilitating seamless transitions and effective collision management during dynamic interactions.

3 Frequency-Based Collision Detection Filter

3.1 Problem Statement

Filtering was not applied to dynamometer measurements during experiments in previous studies on Physical Human–Robot Interactions using the CRAFT prototype [1, 8, 9]. This choice was based on two main considerations. First, collision detection relies on prompt variations in tension measurements, for which direct analog signals were deemed sufficient. Second, the system operates at a high frequency of 1000 Hz to ensure robustness and responsiveness, making the implementation of complex filters computationally challenging within the given time constraints.

In [1], the tension tracking error $\boldsymbol{\delta\tau}$ is defined as an 8-dimensional vector representing the difference between the desired and measured cable tensions:

$$\boldsymbol{\delta\tau} = \boldsymbol{\tau}_m - \boldsymbol{\tau}_d \tag{8}$$

A threshold of 5 N was empirically determined to balance sensitivity and specificity in collision detection [8]:

$$T_h = 5\,\mathrm{N} \tag{9}$$

A collision is detected if any element $\delta\tau_i$ in $\boldsymbol{\delta\tau}$ exceeds the threshold T_h:

$$\exists\ \delta\tau_i \in \boldsymbol{\delta\tau} : \delta\tau_i > T_h \tag{10}$$

However, the cable tension errors $\boldsymbol{\delta\tau}$ were observed to fluctuate around ± 2 N. These oscillations are attributed to measurement noise from sources such as electromagnetic interference and device errors. The presence of high-frequency noise in direct measurements compromises detection accuracy, necessitating either more stringent calibration or the implementation of a detection threshold T_h set to 5 N, which exceeds the measurement error. Furthermore, the direct measurement data exhibit significant peaks and lack smoothness, which can lead to saturation when using the feedback loop. Such saturation adversely affects the control loop's reliability by introducing discontinuities.

3.2 Filter Design and Implementation

To address these challenges, an Exponential Moving Average (EMA) filter was adopted to mitigate high-frequency noise while maintaining responsiveness. The

EMA filter smooths the raw tension measurements $\boldsymbol{\tau}_m$, yielding filtered tensions $\boldsymbol{\tau}_{mf}$:

$$\boldsymbol{\tau}_{mf}(t) = \alpha\ \boldsymbol{\tau}_m(t) + (1-\alpha)\ \boldsymbol{\tau}_{mf}(t-1), \tag{11}$$

where the filtered tension $\boldsymbol{\tau}_{mf}(t)$ at time t is derived from the raw tension measurement $\boldsymbol{\tau}_m(t)$ using a smoothing factor α, which balances responsiveness and noise suppression. A higher α results in a more responsive system but increases signal noise, while a lower α reduces noise but makes the system less responsive.

3.3 Selection of the Smoothing Factor α

The smoothing factor α ensures prompt response to significant tension changes while reducing measurement noise. According to [10], for a first-order low-pass filter:

$$\alpha = \frac{2\pi f_c T_s}{1 + 2\pi f_c T_s}, \tag{12}$$

where $T_s = 1/f_s$ is the sampling interval.

In this approach, the cutoff frequency f_c must balance noise reduction and signal fidelity. Initially, a Fast Fourier transform was applied to sensor measurements recorded in a static pose, revealing that the data were predominantly affected by white noise. In principle, selecting the lowest possible cutoff frequency helps eliminate this high-frequency noise. However, the cutoff frequency must also accommodate the system's significant frequencies to avoid unduly filtering out relevant dynamics.

For the CRAFT prototype, an impulse test indicated a dominant frequency of 3.67 Hz. Using this frequency as a reference, f_c was set to 3.67 Hz, resulting in $\alpha = 0.0236$. This value reflects a compromise: it is low enough to suppress noise yet high enough to capture the essential dynamics of the system as determined under the tested conditions. If the desired motion demands higher frequencies, relying on this cutoff could introduce undesirable oscillations, suggesting that the chosen frequency is closely tied to the physical limits of the system. In future applications, the cutoff frequency may need adjustment depending on the reference trajectory and the operational requirements of the CDPR.

3.4 Experimental Results

Collision tests were conducted to evaluate the impact of different α values on detection performance while employing the EMA filter and adopting a reduced threshold $T_h = 3$ N. EMA filters with $\alpha = 0.01$, 0.0236, and 0.05 were tested. Increasing α from 0.01 to 0.05 raised the collision detection delay from approximately 0.027 s, 0.045 s to 0.075 s. The configuration with $\alpha = 0.0236$ provided a suitable compromise, yielding smoother tension measurements without substantially increasing detection delay, and allowing for a lower threshold to detect collisions more rapidly.

Figure 3 illustrates that implementing the EMA filter with $\alpha = 0.0236$ further enhanced collision detection reliability and accuracy. By effectively reducing

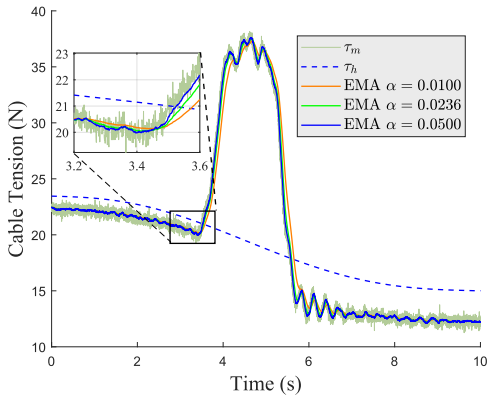

Fig. 3: Comparison of EMA filter parameters and their impact on collision detection delay

noise-induced false positives, this filtering strategy improved the responsiveness of the control system and facilitated quicker collision detection during physical human-robot interactions.

4 Collision Management via Cable Length Release

4.1 Collision Management Strategy

Figure 2 illustrates the safety management strategy for collisions. The approach builds upon the methodology developed in [1], where the detection of the collision and identification of the cable c in collision is detailed. In that prior work, the strategy upon collision detection involves reducing the tension in the identified cable to a safe level and, if necessary, modifying the cable length once. However, due to the non-reversibility of the actuators, the measured tension cannot fully match the desired tension without continuous adjustment of the cable length. This limitation becomes pronounced if contact conditions vary during interaction, as may occur when the robot collides with a human operator.

The present approach addresses this limitation by introducing a closed-loop tension control that, facilitated by the implementation of the EMA filter, continuously adjusts the cable length to ensure that the measured tension follows the desired tension more closely throughout the entire collision duration. The key steps of the initial method in [1] and the enhancements introduced here are summarized as follows:

Collision Detection and Cable Identification: Upon collision occurrence at time t_{col}, the algorithm identifies the cable c involved in the collision, as detailed in [1]. To fully model the tension evolution, knowledge of both the collision onset and collision end times is required. The red detection block in Fig. 2

outputs a vector $\mathbf{v}_{col}$ representing the cable tension profile $\boldsymbol{\tau}_{mf}$ and $\boldsymbol{\delta\tau}$ at t_{col}. To smoothly decrease and restore the maximum tension, a function $s(t)$ is defined, with a transition period of 2 seconds. This duration is chosen to avoid sudden reductions in control input and ensure a gradual decrease in tension. Subsequently, a cable selector matrix **SI** is utilized to differentiate between the collided cable and normally operating cables:

$$\mathbf{SI} = \mathrm{diag}(\delta_{1,c}, \delta_{2,c}, \ldots, \delta_{8,c}), \tag{13}$$

where the Kronecker delta, $\delta_{i,j}$, is defined as 1 when $i = j$ and 0 otherwise.

Gradual Reduction of Maximum Tension and Initial Cable Length Adjustment: In the original approach [1], once the collided cable c is identified, its maximum tension limit $\boldsymbol{\tau}_{\max}$ is reduced in open-loop control, and its length is adjusted to lower tension. To implement this, the management time function $\mathbf{S}(t)$ is obtained by the dot product of $s(t)$ and **SI**, progressively decreasing $\boldsymbol{\tau}_{\max}$ until it reaches the minimum allowable tension $\boldsymbol{\tau}_{\min}$. Concurrently, the adaptive cable release length is calculated via Eq. (14), and the desired joint angle shifts from $\hat{\mathbf{q}}_d$ to $\mathbf{q}_d$. Although this open-loop reduction avoids abrupt tension drops, it may be insufficient under varying contact conditions, potentially resulting in suboptimal collision handling.

Continuous Closed-Loop Tension Control (New Contribution): This continuous cable length control is enabled by the implementation of the EMA filter, which provides smoothed tension measurements necessary for accurate regulation. Consequently, the system can accommodate varying contact conditions during human-robot interaction, ensuring more effective and responsive collision management compared to the single adjustment performed in [1].

Post-Collision Restoration: Following the resolution of the collision, the function $\mathbf{S}(t)$ is updated to incrementally restore the maximum cable tension $\boldsymbol{\tau}_{\max}$ and gradually return the cable length to its default value. This restoration process ensures a smooth transition back to normal operating conditions, mitigating any discontinuities that could compromise the system's reliability. Unlike the single adjustment method in [1], the continuous closed-loop approach supported by the EMA filter facilitates robust and adaptive collision management in dynamic physical human-robot interactions.

4.2 Cable Release Method

In the new control scheme, when a collision is detected on a cable, joint position control is applied to the other seven cables to maintain system position, while tension control is applied to the collided cable to track the minimum desired tension τ_{dmin}, set to 3 N. Defining the tension tracking error as $\delta\tau_f = \tau_{mf} - \tau_{dmin}$, the control loop is expressed as:

$$\delta l_c = K_g T_s \,\mathrm{sgn}_m(\delta\tau_f) + K_e T_s \,\delta\tau_f, \tag{14}$$

where T_s is the sampling period. This control law consists of two parts:

Proportional Correction *($K_e T_s\, \delta\tau_f$):* The first term handles smaller tension deviations. Since it is directly proportional to the tension error, this component ensures a smoother, more gradual response to minor fluctuations. By continuously adjusting δl_c in proportion to $\delta\tau_f$, the controller fine-tunes its response to reach the desired state with minimal steady-state error.

High-Gain Adjustment *($K_g T_s\, sgn_m(\delta\tau_f)$):* This term rapidly corrects significant tension errors, ensuring a quick response to large deviations while ignoring minor fluctuations. By using the modified sign function sgn_m, the controller activates a strong correction only when the tension error exceeds certain thresholds, thus preventing overreaction to negligible changes. The parameter K_g is tuned to achieve the desired responsiveness in adjusting the cable length. Additionally, to model cable elasticity, the elastic parameter K_e is introduced and defined according to Hooke's law:

$$K_e = \frac{l_u}{ES}, \tag{15}$$

where l_u is the undeformed cable length, E is the Young's modulus, and S is the cross-sectional area of the cable. The modified sign function $\mathrm{sgn}_m(\delta\tau_f)$ designed for adaptive gain control and to prevent abrupt changes in the control output during tension error management, ensuring smooth and stable system responses. It is defined as:

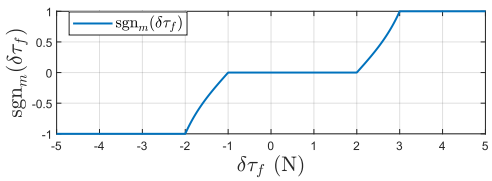

Fig. 4: Piecewise function $\mathrm{sgn}_m(x)$: 1 if $x > 3$; $\tan\big((x-2)\pi/4\big)$ if $2 < x \leq 3$; 0 if $-1 \leq x \leq 2$; $-\tan\big((-x-1)\pi/4\big)$ if $-2 < x < -1$; and -1 if $x \leq -2$.

For large tension errors, $\delta\tau_f < -2$ or $\delta\tau_f > 3$, the term $\mathrm{sgn}_m(\delta\tau_f)$ activates the high-gain component, $K_g T_s\, \mathrm{sgn}_m(\delta\tau_f)$, to rapidly counteract disturbances. Within the transition regions, the control action increases smoothly, ensuring a gradual response and avoiding abrupt changes. For minor variations or noise within the delay zone, $-1 < \delta\tau_f < 2$, $\mathrm{sgn}_m(\delta\tau_f) = 0$ allows the controller to disregard insignificant fluctuations and prevent unnecessary adjustments.

When the collision ends, no external disturbances persist, and the displacement regulation term $K_g T_s\, \mathrm{sgn}_m(\delta\tau_f)$ in Eq. (14) settles into its dead zone, approaching zero. With no ongoing interaction, tension variations vanish due to external force ceasing, causing the cable elongation term $K_e T_s\, \delta\tau_f$ to be sufficiently small and δl_c to remain below 0.1 mm for 1 second. Because any continuous interference (e.g., a human arm still touching the cable) would produce

subtle vibrations and prevent perfect steadiness, the method remains sensitive to genuine collisions. By relying directly on measured tension rather than inferred forces, this new approach achieves both greater precision and faster responsiveness in detecting collision termination.

4.3 Experimental Results

Case 1 In the static experiment, collisions were sequentially triggered with Cables 7 then 5 while the MP was stationary above the stand.[1]

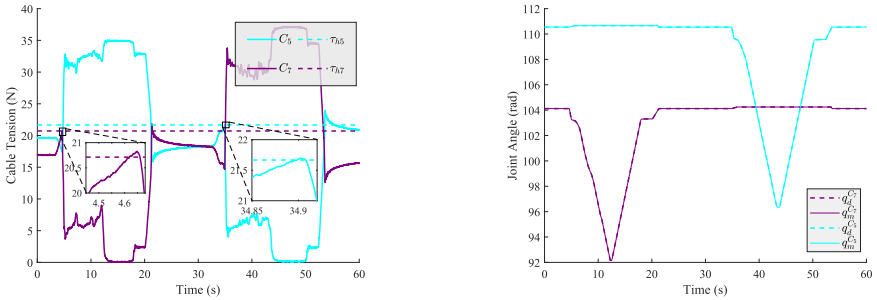

(a) Filtered measured cable tensions ($\boldsymbol{\tau}_{mf}$) and threshold

(b) Desired and measured motor joint angles ($\mathbf{q}_d$ and $\mathbf{q}_m$)

Fig. 5: Results of collisions when the MP is static: human-cable collision first with Cable 7, then with Cable 5. Here, C_j denotes the j^{th} cable of the CDPR, and τ_{hj} denotes the collision detection tension for C_j, where $j = 5, 7$.

Figure 5a illustrates the filtered measured cable tensions for Cable 5 and Cable 7 during collision tests. Human motion applies variable forces on the cables, causing oscillations in tension. As collisions occur, the tensions in the affected cables increase; the collision management algorithm promptly reduces these tensions below the maximum admissible force. The objective is to keep the collided cables' tensions near the targeted τ_{dmin}, with thresholds applied as shown in Fig. 4. When the human ceases applying additional displacement, cable lengths decrease from approximately 12.483 seconds at maximum allowed speed, and the collision ends are detected around 20.133 seconds. Fig. 5b presents the desired and measured motor joint angles of the collided cables, which closely track the desired angles, indicating smooth and effective control during collision management. These results demonstrate the system's ability to detect individual collision events, maintain cable tensions within allowable limits, and ensure stable platform positioning through adaptive tension redistribution.

[1] Experiment videos are available at https://uncloud.univ-nantes.fr/index.php/s/77jxbBH72i6ib6P.

Case 2 In the dynamic experiment, a collision was triggered with Cable 7 while the MP followed a trajectory as shown in Experiment 2 of the supplementary video.

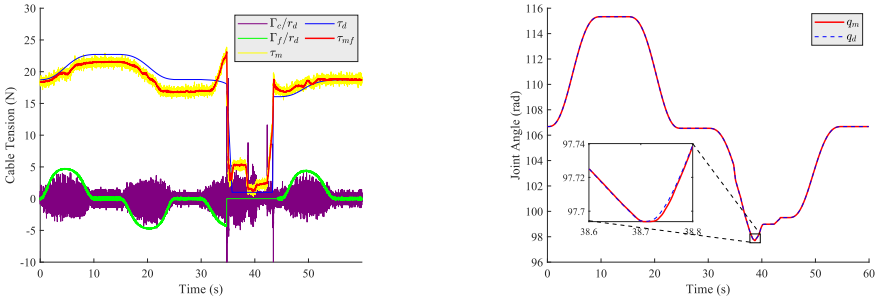

(a) Cable tensions ($\boldsymbol{\tau}$) and motor torques ($\boldsymbol{\Gamma}$)

(b) Desired and measured motor joint angles ($\mathbf{q}_d$ and $\mathbf{q}_m$)

Fig. 6: Results of collisions when the MP is moving: human-cable collision with cable 7.

Figure 6a shows Cable 7 colliding during dynamic motion.Upon collision detection, the desired cable tension was reduced to the minimum allowable tension and the friction compensation was blocked. The tension profile shows the effectiveness of the collision management algorithm, with tension decrease upon collision detection and restoration after collision end occurring within 1 s and 2 s, respectively. Fig. 6b presents the desired and measured motor angles for the collided cable. The motor angle closely tracks the desired trajectory, with a maximum error of 0.0006 rad (about 0.5 mm in cable length), underscoring the algorithm's efficacy.

5 Conclusion

This paper presents significant advancements in the detection, management, and recovery of human-cable collisions in CDPRs. A novel frequency-based filter was introduced for dynamometer measurements, enhancing collision detection accuracy and strengthening the closed-loop feedback in the control scheme. An adaptive control approach for cable length release optimizes collision management in dynamic human-robot interactions, effectively handling both severe and minor collisions. Additionally, a robust collision-end detection method and post-collision recovery strategy ensure efficient restoration of cable tension and length.

Experiments conducted with the CRAFT prototype validated these improvements, demonstrating substantial enhancements in safety and responsiveness during physical human-robot collaboration. The proposed methods contribute

to the advancement of safe human-robot interaction in CDPR systems, marking a significant progression in collaborative robotic environments.

Future research will focus on extending these techniques to handle human-cable collisions outside the feasible workspace, where the remaining seven cables are insufficient to support the moving platform. Additionally, exploring adaptive strategies for dynamic environments and integrating advanced sensing technologies will enhance the system's robustness and applicability in diverse industrial settings requiring human-robot collaboration.

Acknowledgment

This work was supported by both ROBOTEX 2.0 (Grants ROBOTEX ANR-10-EQPX-44-01) and TIRREX (ANR-21-ESRE-0015). The first author is funded by the China Scholarship Council (Grant no. 202208070012). Assistance provided by M. Marceau Métillon through the experiments is highly appreciated.

References

1. Gao, H., Chevallereau, C., Caro, S.: Detection and management of human-cable collision in cable-driven parallel robots. IEEE Robotics and Automation Letters **9**(12), 11698–11705 (2024). https://doi.org/10.1109/LRA.2024.3487051
2. Zarebidoki, M., Dhupia, J.S., Xu, W.: A review of cable-driven parallel robots: Typical configurations, analysis techniques, and control methods. IEEE Robotics & Automation Magazine **29**(3), 89–106 (2022)
3. Xiong, H., Cao, H., Zeng, W., Huang, J., Diao, X., Lu, W., Lou, Y.: Real-time reconfiguration planning for the dynamic control of reconfigurable cable-driven parallel robots. Journal of Mechanisms and Robotics **14**(6), 060913 (2022)
4. An, H., Yu, D., Xu, W., Yuan, H.: Modeling and cooperation method for movable anchor winch cable-driven parallel robot. IEEE/ASME Transactions on Mechatronics pp. 1–12 (2024). https://doi.org/10.1109/TMECH.2024.3478357
5. Sun, C., Gao, H., Liu, Z., Xiang, S., Yu, H., Li, N., Deng, Z.: Design of spatial adaptive cable-driven parallel robots with an unlimited rotation axis using the cable wrapping phenomenon. Mechanism and Machine Theory **171**, 104720 (2022)
6. Xiong, H., Xu, Y.: Statics and path of the cables of a cable-driven parallel robot wrapping on surfaces. In: International Conference on Cable-Driven Parallel Robots. pp. 82–94. Springer (2023)
7. Xiong, H., Xu, Y., Yu, Y., Lou, Y.: Cable path analysis and kinematic control of a cable-driven parallel robot allowing cables to wrap on cylinders or spheres. Journal of Mechanisms and Robotics **17**(1) (2025)
8. Rousseau, T., Chevallereau, C., Caro, S.: Human-cable collision detection with a cable-driven parallel robot. Mechatronics **86**, 102850 (2022). https://doi.org/10.1016/j.mechatronics.2022.102850
9. Métillon, M., Charron, C., Subrin, K., Caro, S.: Performance and interaction quality variations of a collaborative cable-driven parallel robot. Mechatronics **86**, 102839 (2022). https://doi.org/10.1016/j.mechatronics.2022.102839
10. Proakis, J.G., Manolakis, D.G.: Digital Signal Processing: Principles, Algorithms, and Applications, chap. 6, p. /* Insert specific page numbers if available */. Pearson, 4th edn. (2014), section 6.2: First-Order IIR Filters